Video Article

Tip-Enhanced Raman Spectroscopy (TERS) Imaging of Grapheme

Andrew Pollard[1], Naresh Kumar[1], Weitao Su[2], Debdulal Roy[1]

[1]National Physical Laboratory

[2]Institute of Material Physics, Hangzhou Dianzi University

Correspondence to: Andrew Pollard at andrew.pollard@npl.co.uk

URL: http://www.jove.com/video/51722
DOI: doi:10.3791/51722

Keywords: graphene, tip-enhanced Raman spectroscopy, TERS, nanoscale imaging, characterisation, defects, 2-D material.

Date Published: 3/31/2014

Citation: Pollard, A., Kumar, N., Su, W., Roy, D. Tip-Enhanced Raman Spectroscopy (TERS) Imaging of Grapheme. *J. Vis. Exp.* (), e51722, doi:10.3791/51722 (2014).

Abstract

The supreme properties of graphene and the potential of this two-dimensional (2-D) material for applications in many different areas of technology have been well-documented over the last decade, and many different techniques are used to characterise this allotrope of carbon. Raman spectroscopy is commonly seen as the technique of choice for characterising both the physical and chemical properties of this material, and tip-enhanced Raman spectroscopy (TERS) can provide this information with nanoscale lateral resolution. This is achieved by employing a nanoscale-sharp metal tip to enhance the electromagnetic field of the incident laser at the end of the tip. This combination of Raman spectroscopy and scanning probe microscopy (SPM) leads to the enhancement of the Raman signal in an area of the order of nanometres, thus providing both high chemical sensitivity and nanoscale spatial resolution. However, it can be difficult to obtain reliable experimental results using TERS, due to the required expertise in both Raman spectroscopy and SPM and the need to overcome obstacles such as the preparation of reproducible TERS probes. However, when these obstacles are overcome, TERS is an exciting technique for graphene research as it can be used to increase the understanding of both graphene itself, through nanoscale surface mapping, and fundamental Raman spectroscopy analysis of graphene layers, typically seen as the 'gold standard' of graphene characterisation.

In this paper, we detail the methodology of how to achieve nanoscale TERS imaging of graphene surfaces, covering aspects such as optical alignment and tip preparation. Typical problems both before and during imaging are described, as well as possible solutions. Finally, TERS imaging of mechanically exfoliated graphene is shown, and the methods of analysing this data are discussed.

Introduction

The potential of graphene to become the next disruptive technology has been frequently presented in scientific journals over the last several years[1-3], and the attention this two-dimensional (2-D) material has enjoyed has also proliferated to many other forms of media as well, due to its many exciting properties. This honeycomb network of sp^2-hybridised carbon atoms, that is just one atom thick, has also initiated research into a whole range of other new 2-D materials, such as hexagonal boron nitride (hBN) and molybdenum disulphide (MoS_2)[4-6]. The many wondrous and unique properties of graphene, such as stiffness, tensile strength, and electrical and thermal conductivity[1, 2, 7, 8] have led to the prediction of many commercial applications for this material over the next decade, in areas such as flexible electronics, photonics, composites, energy storage and sensors[3].

Raman spectroscopy is a key technique for characterising the properties of graphene[9, 10] and provides a wealth of chemical, electrical and structural information. Raman spectroscopy can be used to determine the number and orientation of layers[11, 12], strain[13, 14], lattice disorder[15, 16] and doping[17, 18] present in graphene, as well as identify chemically bound species present in functionalised graphene[19]. By using an excitation laser to excite the inelastic Raman scattering processes in graphene, and measuring the resulting change in frequency of the scattered photons using a monochromator, samples can be rapidly analysed. The technique is also non-destructive when the laser power density incident on the graphene surface is less than 1 mW over a 1-2 µm spot diameter[20]. Confocal Raman spectroscopy can also be used to spatially map graphene layers by rastering the focus of the excitation laser across the sample and thus determine the variation in properties over the graphene surface. However, the lateral resolution of this technique is limited by the diffraction limit (λ/2NA, where NA is the numerical aperture) to several hundred nanometres, depending on the wavelength of the excitation laser. Tip-enhanced Raman spectroscopy (TERS)[21] has been shown to provide an improvement in lateral resolution by more than one order of magnitude, with sub-molecular resolution of < 1 nm recently achieved on a single molecule[22]. The benefits of using TERS to image graphene rather than far-field Raman spectroscopy has already led to the measurement of the phase-breaking length at graphene edges[23] and the localisation of graphene defects at a resolution higher than the optical diffraction limit[24]. TERS is achieved by utilising a sharp metallic scanning probe microscopy (SPM) probe to strongly enhance the electric field at the tip apex and thus produce an enhancement of the Raman signal in a localised nanoscale area. In a TERS setup, the excitation laser wavelength is chosen so as to excite localised surface plasmons at the metallised tip apex[21]. Typically, either gold or silver tips are used in combination with red or green laser light, respectively. Ultimately, the success of any TERS measurement relies on the probe used, with many variations of tip fabrication possible. However, the range of TERS tips available is limited, depending on both the SPM feedback mechanism used (as this probe must follow the topography of the surface) and the type of sample under investigation.

Scanning tunnelling microscopy (STM)[25] tips can be used for measuring conductive samples, whereas atomic force microscopy (AFM)[26] cantilevers are employed for, but not limited to, non-conducting samples. Further choices can be made as to whether contact-mode AFM, where the tip is in contact with the surface and the deflection of the cantilever is monitored[23], or an oscillating cantilever[27] should be employed. STM

tips are usually electrochemically etched from thin metal wire, which can produce a tip apex with a nanoscale radius of curvature. Etched gold or silver wires can also be used for AFM tips[28, 29], if it is then secured onto a cantilever assembly, typically a quartz tuning fork, that may then be used in shear force mode[30] or tapping mode AFM[31].

In this body of work, we describe the TERS mapping of mechanically exfoliated graphene using a silver-coated AFM tip in contact-mode specifically. These tips were produced by oxidising commercially available silicon AFM contact-mode cantilevers to provide a supporting dielectric substrate for a silver film, coated using thermal evaporation in a vacuum of ~10^{-6} mbar[32, 33], to achieve surface plasmon resonance with 532 nm wavelength excitation. Although the oxidation of the cantilever is not a requirement, it does improve the surface-enhanced Raman scattering at the TERS probe apex. An AFM system was mounted on an inverted confocal microscope and a radially polarised 532 nm excitation laser beam was used to illuminate the AFM tip apex from below the transparent sample. This transmission-mode setup is shown in Figure 1. The 1.49 NA oil-immersion objective lens used for the incident laser beam also collected the Raman scattered light, which travelled to the Raman spectrometer and a charge-coupled device (CCD) detector via a multimode fibre with a core diameter of 25 µm. To minimise vibrational and acoustic noise and undesired illumination, the entire apparatus was enclosed and placed on an optical table with passive isolation. The TERS results were acquired and displayed using a combination of SPM and spectroscopy software in a master-slave configuration respectively. Key challenges in performing TERS measurements are the production and stability of the TERS probes, as well as the issue of spurious results due to tip contamination. To this end, particular care must be taken to avoid adventitious contamination and to verify any unexpected spectra.

Protocol

1. Laser and Raman Signal Alignment

1. Align the laser beam through a spatial filter to remove any intensity variations and other inhomogeneities. Then pass the collimated beam from the spatial filter through a radial polariser (Figure 1b). Align the optical setup so that the laser beam will enter the exact centre of the objective lens to achieve the best diffraction limited focal spot on the sample, then secure the objective lens onto the microscope. NOTE: To obtain a diffraction limited focal spot, a collimated beam must be achieved using a spatial filter, as shown in Figure 1b. By including a radial polariser, a higher z-component of the electric field can be obtained in the focal plane of the laser spot[34].
2. Clean the oil immersion objective lens using isopropanol and a lens cleaning tissue in one sweeping motion. Place a laser power meter in the sample position and adjust the output power of the laser system so the power measured at the objective lens is approximately 0.3 mW. Apply fresh oil to the objective lens using an oil dropper.
3. Place a 0.17 mm thick (thickness number – 1½) glass coverslip in the sample position and add a small amount of oil to the top of the coverslip before securing a silicon wafer on top of the coverslip, front (polished) side facing downwards. Allow 20-30 minutes for the oil to settle before any measurements are performed.
4. Calibrate the spectrometer using the corresponding control software, adjusting the calibration offset until Raman spectroscopy measurements show a Rayleigh scattering line at 0 cm^{-1} and then adjusting the calibration coefficient so that the first order silicon Raman peak is positioned at 520 cm^{-1}.
5. Maximise the silicon Raman peak by adjusting the focus of the laser beam, using the optical microscope focus knob, and align the confocal pinhole of the 25 µm multimode fibre collecting the Raman scattered light by adjusting the lateral positioner of the fibre situated on the inverted microscope.

2. TERS Tip Preparation

1. Place silicon contact-mode AFM cantilevers without any metal back-coating (see Materials Table) in a tube furnace. Set the temperature of the tube furnace to 1000˚C and, once the desired temperature is reached, pass steam over the AFM tips by boiling water in a connected, sealed vessel for ~45 minutes. NOTE: On completion, the cantilevers should have a purple or green colouration indicating a thickness of greater than 300 nm oxide layer grown on the silicon material.
2. Place the oxidised TERS probes in a UV ozone cleaning chamber for one hour to remove any organic contamination.
3. Place the oxidised tips in a high-vacuum thermal evaporator system (vacuum pressure of ~10^{-6} mbar). Increase the temperature of a molybdenum evaporation boat containing silver material until a slow evaporation rate of ~50 pm/s is achieved, as measured using a calibrated quartz crystal microbalance. Deposit a 40-50 nm nominal thickness silver film on the TERS probes. Store the batch of TERS probes in an argon (or nitrogen) atmosphere until they are needed.

   NOTE: To produce usable TERS tips, care must be taken to keep the evaporation system free of carbon contaminants, which will lead to unreliable results. TERS tips should be used within a few days of preparation and ideally be prepared on the same day to reduce both oxidation and contamination of the silver coating. An SEM image of a TERS probe is shown in Figure 2c.

3. Mechanically Exfoliating Graphene Flakes

1. Rinse a 0.17 mm glass coverslip with ethanol and dry the coverslip using a nitrogen or argon spray gun. Clean the substrate in a UV ozone cleaning chamber for 10 minutes.
2. Cover one side of a highly oriented pyrolytic graphite (HOPG) surface with adhesive tape. Make sure the tape is in contact with the entire HOPG surface securely by pressing down on the tape with tweezers. Peel off the tape to reveal graphite layers on the tape itself.
3. Spread the graphite layers across the adhesive tape by sticking the tape together and peeling the tape apart several times. Then cover the clean glass coverslip with a part of the adhesive tape where graphite layers are present, pressing gently on the tape with tweezers to make sure it is securely in contact with the glass coverslip. Slowly peel the adhesive tape off of the glass coverslip to produce flakes of graphite and graphene on the glass coverslip.

NOTE: The graphene layers on the glass surface will be undetectable to the naked eye.

4. Performing TERS Measurements on Graphene:

1. Use the inverted microscope to identify an area on the glass coverslip where there is a visible graphite flake. Perform low-resolution confocal Raman mapping in this location over an image area tens of microns in size. Analyse the Raman spectra obtained to identify a graphene area of interest. For a graphene monolayer area (preferably several hundred nanometres in lateral dimensions) identify any Raman spectra containing a sharp Lorentzian 2D-peak at ~2670 cm^{-1} with a greater Raman intensity than the G-peak at ~1590 cm^{-1}, as shown in the Raman spectra in Figure 3c labelled 'centre'.
2. Use a sacrificial TERS tip that will not be used for any further TERS measurements to first position the AFM feedback laser with respect to the TERS cantilever. Roughly align the TERS tip with the centre of the excitation laser focus using the AFM XYZ coarse tip positioning system. Approach the contact-mode tip towards the sample surface using the AFM system software to step the coarse tip Z-positioning motor whilst varying the fine sample Z scanner.
3. Once the AFM approach procedure has finished, confirm that the cantilever deflection is stable and thus the AFM contact-mode feedback is performing correctly. Determine the optimum deflection setpoint for reliable feedback, which minimises the force applied to sample by the TERS tip, by reducing the deflection setpoint until the feedback becomes unstable and then increasing the deflection setpoint until the cantilever deflection is stable again.
4. Replace the sacrificial TERS probe with a new TERS tip that has been prepared within the last few days, or preferably the same day. If required, re-align the AFM deflection laser with the back of the new AFM cantilever and re-align the tip position with the laser focus using the XYZ coarse tip positioning motors. To improve the alignment of the focus of the excitation laser with the tip apex, perform XY Raman mapping of the tip using the objective lens XYZ scanner and position the beam focus at the point of maximum Raman intensity for the silicon (~520 cm^{-1}) peak, as shown in Figure 2a.

   NOTE: Depending on the thickness of the oxide layer, the Si peak may not be observable using Raman spectroscopy. In this case the maximum of the photoluminescence (PL) intensity from the silver coating can be used to roughly align the tip with the centre of the laser focus.
5. Approach the identified graphene layers with the TERS probe until it is in AFM contact-mode feedback, using the previously determined approach parameters in Step 4.2 to minimise the force on (and therefore the tip degradation of) the TERS tip. Perform further Raman imaging of the tip using the objective lens XYZ scanner once the probe is in contact with the graphene flake. Determine the position of the graphene Raman G-peak maximum intensity, and align the excitation laser with this TERS 'hot-spot', that is, the location of the centre of the Raman signal enhancement, as shown in Figure 2b.
6. Record the Raman spectra both when the TERS probe is in contact with the graphene surface, and when both the sample and objective lens are simultaneously retracted from the probe (thus the excitation laser focus is still positioned at the same sample location). If a graphene G-peak contrast of 1 or higher is achieved, as for the example in Figure 2d, position the TERS tip onto the graphene surface again. Allow the system to stabilise for 10 minutes and then perform Raman mapping using the XYZ objective lens scanner on the TERS tip again to determine if any re-alignment of the TERS hot-spot is required.

   NOTE: This step is described as a 'Tip in/Tip out' experiment and can be used to determine the TERS contrast of the TERS tip, and if it is usable for TERS measurements. For a contrast of less than 1, the TERS hot-spot should be re-aligned and another Tip in/Tip out experiment performed to assess the TERS probe. If a suitable contrast value is still not achieved, a new TERS probe should be employed and the protocol should be followed from Step 4.4.
7. Set the AFM software to record the topography, lateral force, and deflection AFM signals as well as the Raman spectra input from the Raman spectroscopy software, at each pixel. Perform TERS imaging of the graphene surface by using the AFM software to execute an AFM map of the area and control the Raman spectroscopy software to acquire Raman spectra at each pixel. NOTE: Typically Raman spectroscopy collection times of 1-2 seconds per pixel are adequate for obtaining graphene Raman spectra. Representative simultaneous lateral force and Raman spectra maps are shown in Figure 3a and 3b respectively and were obtained by laterally displacing the surface using the sample XYZ scanner relative to both the objective lens and TERS probe.
8. When TERS measurements show areas of scientific interest, repeat the TERS imaging procedure in Step 4.7 to prove measurement consistency, imaging the areas at different scan sizes to confirm the features observed. NOTE: A Raman spectral measurement of the TERS tip can also be performed when it is not in contact with the surface, to determine if any contamination has been acquired by the tip that may have produced any spurious results in any previous scans.
9. When a reduction in the lateral resolution of the TERS tip is observed in the tip-enhanced Raman image, re-scan for the graphene G-peak hot-spot using the objective lens XYZ scanner whilst the tip is in contact with a continuous graphene flake. If the hot-spot is not a sharp point, or several hot-spots are found, as shown in Figure 2e and 2f, the tip should be replaced as the silver coating has been damaged at the tip apex.
10. Replace the TERS tip with another recently prepared TERS tip (or one that was recently stored in an argon atmosphere). Repeat steps 4.3 to 4.7 to determine if the new TERS tip is performing correctly and to re-image the previous areas measured. NOTE: The consistency of any experimental TERS results obtained is demonstrated by performing TERS imaging with different TERS probes on the same sample area.

Representative Results

Figure 1 illustrates the experimental TERS apparatus, in which Figure 1a is a detailed view of the silver-coated AFM tip in contact with a graphene layer on a glass coverslip. The green laser beam is incident on the probe apex and thus the sample, with Raman scattered light emanating from the sample. Some of the scattered Raman signal is collected by the same objective lens that focusses the excitation laser beam. Figure 1b shows a schematic view of the experimental equipment, including the optics required for a collimated and radially polarised beam and the Raman spectrometer with associated CCD camera that measures the collected Raman scattered light.

Raman intensity maps of a TERS probe are shown in Figure 2a and 2b, which illustrate that the maximum signal found for the silicon peak of the AFM cantilever tip (Figure 2a) is not in the same location as the true TERS hot-spot, found from the graphene Raman G-peak intensity map in Figure 2b. Both Raman intensity maps of TERS probes, such as in Figure 2a and 2b, and TERS intensity images of samples are, by their nature, a superposition of both the TERS signal at the hot-spot and far-field Raman spectroscopy signal from the overall laser probe volume. Thus, the contrast between the near-field and far-field signals can be used to characterise TERS tips by performing 'Tip in/Tip out' experiments, as described in the Protocol section, and using the formula $I_{near}/I_{far} = (I_{in}/I_{out}) - 1$. Figure 2c is a scanning electron microscopy (SEM) image of a silver-coated AFM cantilever, clearly showing a tip apex radius of less than 50 nm and the required rough silver surface produced by this tip production method for efficient excitation of localised surface plasmons. When developing a fabrication procedure for TERS probes, the characterisation of the tip apex is extremely important to confirm the viability and reliability of the tips. Although much higher contrasts have been reported[23, 24], a functioning TERS probe will produce a contrast of at least ~1 for Tip in/Tip out experiments on graphene, as shown in the example in Figure 2d for a monolayer graphene layer after Ar^+ ion bombardment. Ion bombardment of graphene causes lattice defects and activates a Raman D-peak[16] at ~1350 cm^{-1}, thus Figure 2d provides a good representation of Raman spectra for defective graphene. The Raman spectra in Figure 2d were obtained when the tip was in contact with the sample surface (Tip in) and when the tip was then retracted by 10 µm from the sample, whilst the excitation laser focus was maintained on the same area of the sample, and Raman spectroscopy measurements repeated (Tip out). This provides an indication of TERS contrast, that is, a quantification of the enhancement of the Raman signal due to the TERS probe.

The silver-coated TERS contact-mode probe typically has a finite imaging lifetime, after which the TERS enhancement drastically reduces as the metal-coating of the tip apex has physically degraded. The domain size of photovoltaic polymer blends are often characterised using TERS imaging[35], and have a reduced measure of hardness compared to a graphene/glass surface. Figures 2e and 2f are Raman maps of a contact-mode TERS probe in contact with a photovoltaic polymer blend of SiTPT-BT and an**indene-C_{60}** monoadduct (ICMA) fullerene-derivative, showing the intensity of the 655 nm photoluminescence peak of the SiTPT-BT polymer. Figure 2e shows the initially sharp hot-spot observed for the TERS probe and Figure 2f reveals that even this softer polymer blend sample damages the tip, and ultimately diminishes the TERS hot-spot, after 4 hours of TERS imaging.

Figures 3a and 3b show a lateral force image and a corresponding graphene D-peak intensity plot of the edge of a monolayer graphene flake on a glass coverslip respectively. The number of graphene layers can be determined by the 2D-peak, in this case a single sharp peak shape (see Figure 3b) is observed for the graphene flake on the left-hand side of the lateral force image in Figure 3a, characteristic of a graphene monolayer[11]. The edge of the graphene flake is observed in Figure 3b as an area of increased D-peak intensity, and shows agreement in the lateral position of the graphene edge with Figure 3a. Figure 3c shows Raman spectra from the areas illustrated in Figure 3b, a point on the graphene flake, on the bare glass substrate and on the edge of the graphene flake. This reveals the absence of significant graphene peaks for the glass substrate, and the difference in the D-peak intensity between the pristine graphene and the edge of the flake, as well as displaying a lateral resolution not achievable with confocal Raman spectroscopy. This is shown in Figure 3d, which is the spatial profile of the graphene G-peak across the edge of the graphene flake, and corresponds to the black horizontal line in Figure 3b.

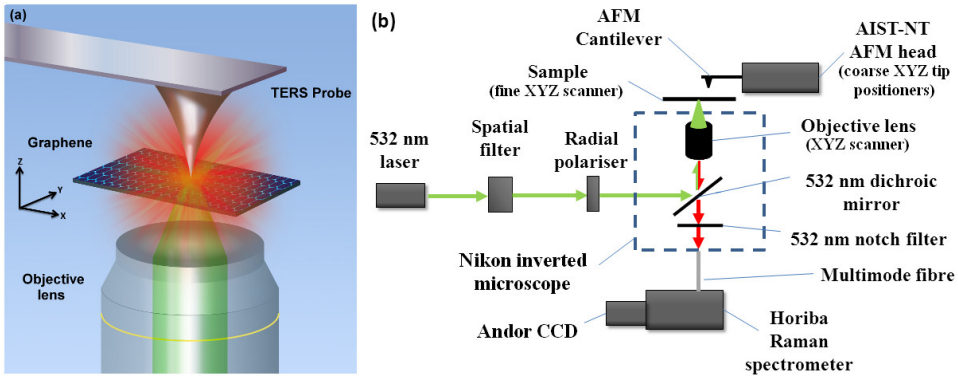

Figure 1: (a) Schematic of a transmission-mode TERS setup using a silver-coated AFM cantilever to map mechanically exfoliated graphene on a glass coverslip. The green laser beam is focussed on the tip apex from below the transparent sample and the Raman scattered light (shown as red) is collected by the same objective lens, the directions of the X-, Y- and Z-axis are also shown. (b) Diagram showing the experimental apparatus of the TERS system, including the optics used for the excitation laser, the AFM head, the inverted microscope, and the Raman spectrometer and charge-coupled device (CCD) camera combination.

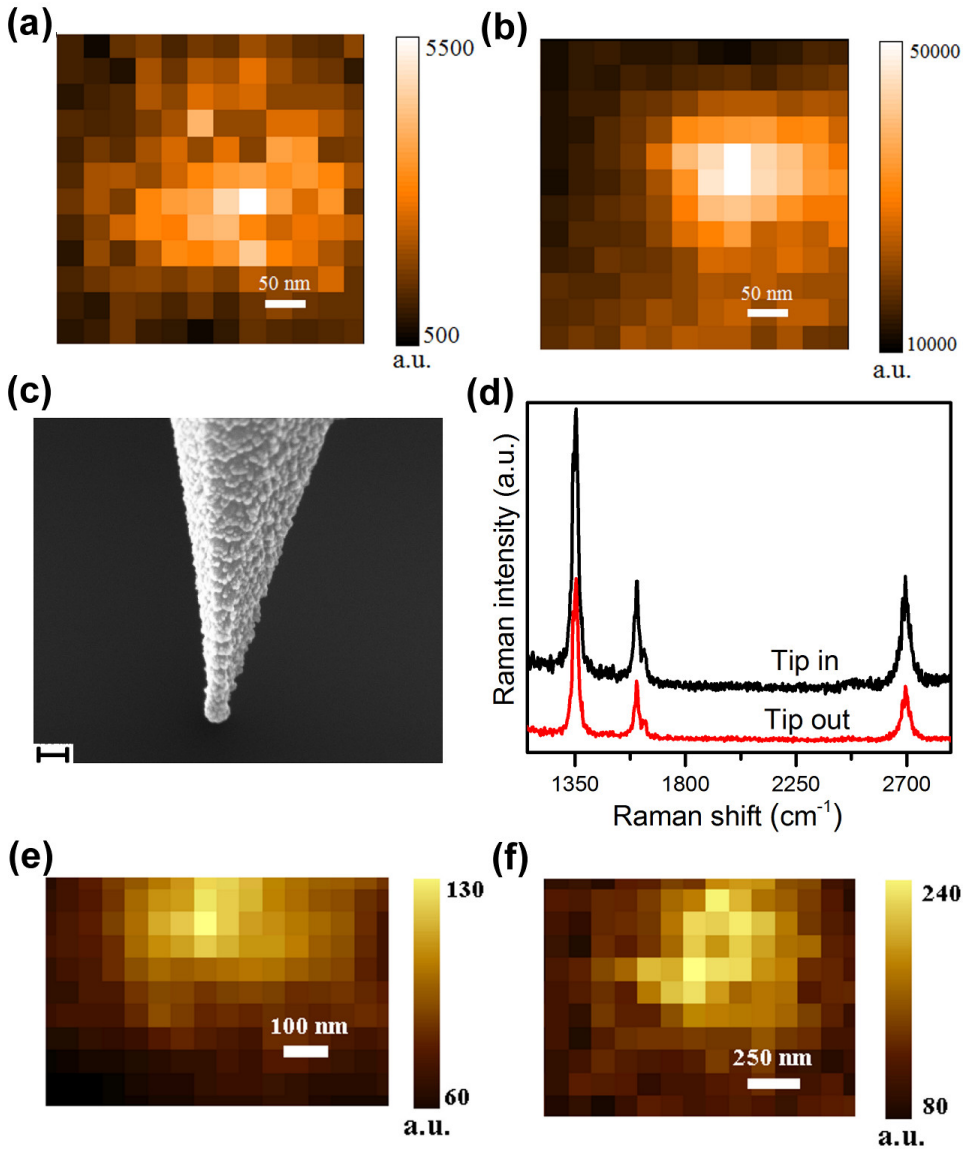

Figure 2: Confocal Raman spectroscopy mapping of a TERS tip in contact with a continuous graphene flake, where (a) and (b) are the silicon (~520 cm^{-1}) and graphene G-peak (~1590 cm^{-1}) Raman maps respectively, pixel size is 37 nm and the z-scale represents the peak area. The true TERS hot-spot in (b) is not at the same location as where the maximum silicon signal is located in (a). (c) SEM image of a ~50 nm silver-coated, oxidised, silicon AFM tip, 100 nm scale bar. (d) 'Tip in' (black) and 'Tip out' (red) spectra for a useable TERS probe at the same lateral position on a graphene monolayer after 500eV Ar^+ ion bombardment and thus a high intensity D-peak is observed. Figure 2d shows the enhancement of the Raman spectra when the TERS tip is in contact with the graphene surface, compared to when the tip has been removed. Raman spectroscopy images of the TERS hot-spot of a probe in contact with a polymer blend sample, before (e) and after (f) the tip has been used. Figures 2e and 2f show how the tip has become blunt after imaging the surface and will not produce significant TERS enhancement. Note (e) is a smaller scan area than (f), with 58.75 nm and 125 nm pixel sizes respectively.

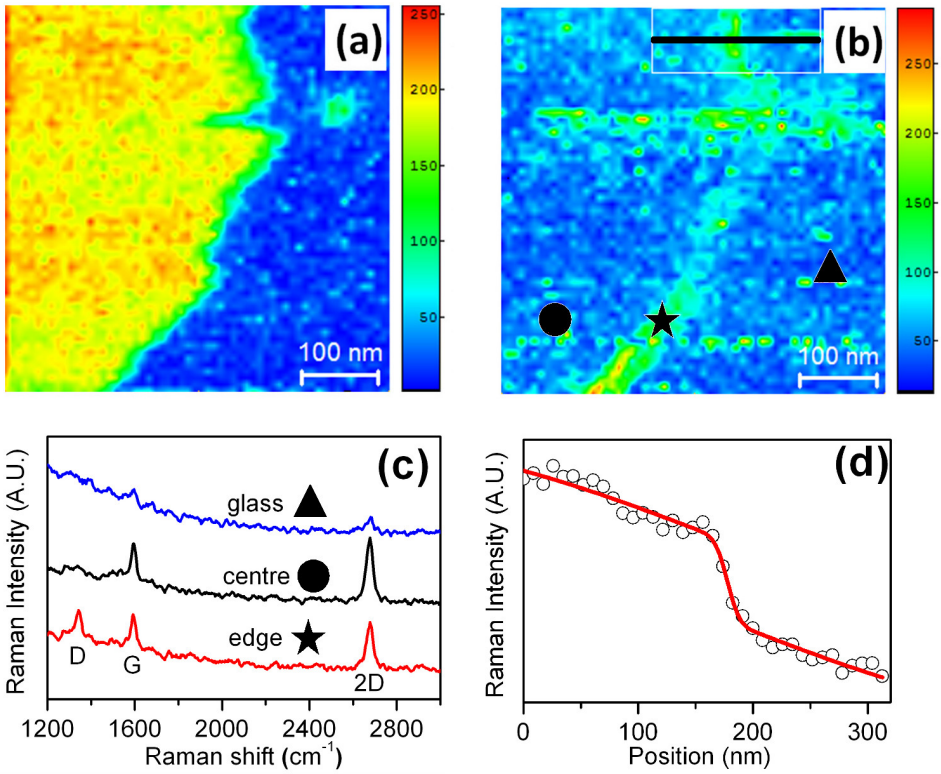

Figure 3: Lateral force (a) and graphene Raman D-peak intensity (b) maps of the edge of a monolayer graphene flake (scan size 500 x 500 nm with 60 x 60 pixels). (c) shows the Raman spectra for the bare glass substrate (triangle), centre of the graphene flake (circle) and the very edge of the graphene flake (star). The graphene flake is clearly distinguishable on the left-hand side of the lateral force image, and the corresponding high intensity D-peak areas are observed in the Raman spectra due to the edge of the graphene flake. Figure 3d shows a profile of the graphene G-peak across the edge of the flake, and corresponds to the black horizontal line in Figure 3b. Reprinted with permission from Ref. 23. Copyright 2013, American Vacuum Society.

Discussion

TERS can be a challenging technique for producing consistent and reliable results and a thorough methodology is required to achieve the desired goals of any TERS experiment. As previously detailed, certain experimental procedures are crucial to confirming any nanoscale-resolution Raman spectra produced by this method. To this end, the apparatus discussed in this body of work allows both the optimisation of the excitation laser and the ability to analyse the viability of the TERS probe *in-situ*.

The AIST-NT AFM head, shown in Figure 1b, has a separate positioning system for the AFM cantilever and for scanning the objective lens, which means that Raman mapping can be performed on the TERS probe itself, or the laser beam can be focussed at a point relative to the tip and the TERS probe and excitation laser focus can be rastered across the graphene sample for TERS imaging. This means the crucial step of locating the TERS hot-spot is easy to accomplish, as is re-alignment, and confirming the position of the hot-spot does not disturb the system if it is already aligned and in the correct position with respect to the sample. Hence the TERS hot-spot can be monitored in-between sample scans, such that damage to the tip due to contact-mode AFM operation (as shown in Figures 2e and 2f) can be investigated and the tip can be rapidly replaced. If, unknown to the user, the TERS probe stops producing an enhancement of the Raman signal, instead of TERS images the user will only be producing confocal Raman maps coupled with AFM data.

Analysis of Figure 2a and Figure 2b reveals that there is a ~56 nm displacement between the maximum silicon Raman peak intensity and the true TERS hot-spot. This is due to local inhomogeneities in the surface roughness present at the tip-apex. This means that although the maximum silicon peak intensity can be used to locate the approximate position of the TERS probe apex before the TERS tip approaches the surface, it is critical to obtain a second Raman map of a Raman peak associated with the sample material itself, when the tip is in contact with the surface. Then the laser focus can be correctly positioned at the TERS hot-spot for maximum enhancement before TERS measurements are undertaken. A functioning TERS probe will reveal a contrast of at least 1, calculated from Tip in/Tip out experiments on graphene, as shown in Figure 2d for a graphene monolayer with a high intensity D-peak caused by Ar^+ ion bombardment[16]. Contrast is a more relevant measure in TERS imaging experiments than 'TERS enhancement factor' values which include an approximation of the difference in probe volumes between confocal Raman measurements and TERS measurements. The Tip in/Tip out measurements in Figure 2d clearly show that there is an enhancement of the graphene Raman signal when a TERS tip is present, and is a necessary step to ensure nanoscale chemical imaging.

Spurious Raman spectra caused by adventitious contamination of the tip is a common cause of suspect results in TERS measurements. The most effective way of addressing this issue is to scan the same area multiple times and at different scan sizes, as described in the protocol previously. TERS tips can easily be replaced without disruption to the sample-objective alignment, allowing the same area of a graphene surface

to be imaged with more than one tip. This robust methodology can therefore confirm the presence of any species imaged on a graphene surface. It is also important to control the laser power incident on the tip and sample since graphene may otherwise be oxidised or react with adsorbates, this is even more of a consideration with TERS than confocal Raman spectroscopy, due to the enhanced localised electric field.

Raman spectra of graphene layers provide several distinctive peaks from which material properties can be discerned. The three most studied bands are the G-peak (~1590 cm^{-1}), the D-peak (~1350 cm^{-1}) and the 2D-peak, which is the D-peak overtone, as shown in Figure 2d and 3c. The D-peak is only activated if there is a defect in the lattice, and thus the ratio of the D- and G-peaks can be used to determine the extent of the disorder in the graphene lattice. The D/G peak intensity ratio increases with increasing defect density until the maximum interdefect distance is ~2-4 nm[16], related to the phase-breaking length of graphene, L_σ[23]. Domain boundaries and edges are both essentially defects in a graphene lattice, and thus an edge of a graphene flake has an increased D-peak intensity depending on the angle of the edge with respect to the graphene lattice. This is observed in Figure 3b as a variation in D-peak intensity along the graphene edge.

There is a convolution of the confocal Raman signal and the nanoscale variations in Raman signal due to the enhancement mechanism of the TERS probe for any TERS experiments. This is the reason the 2D-peak can still be observed in Figure 3c for the bare glass areas, even though the intensity is very small. By analysing the TERS image in Figure 3b with a line profile across the graphene edge and plotting the variation in the graphene Raman G-peak, as shown in Figure 3d, a TERS resolution of 16 nm can be determined[23]. The tip radius of the TERS probe itself also leads to further convolution for surface features that are smaller than the TERS tip apex. However, this can be mathematically deconvoluted, as shown in Ref. 23 where the phase-breaking length of graphene is calculated as $L_\sigma = 4.2 \pm 0.5$ nm from the graphene Raman D-peak image shown in Figure 3b.

As outlined previously, there are several other modes of TERS that incorporate other AFM feedback modes with oscillating cantilevers or STM feedback. However, the Raman signal obtained in contact-mode AFM typically has a more advantageous signal-to-noise ratio as opposed to other AFM feedback modes, whilst the disadvantage of contact-mode TERS is increased tip degradation. STM feedback would not be possible for mechanically exfoliated graphene layers on glass due to the inability to make an electrical contact with microscale transparent graphene flakes. However, STM feedback could be employed with similar samples by incorporating a thin-film of metal deposited on the glass coverslip before the graphene is transferred onto the substrate, this metal can be the same metal as the TERS tip, thus enabling gap-mode measurements[24]. Another option would be to change the optical apparatus from a transmission-mode system, as outlined in this body of work, to a reflection-mode TERS setup that employs an excitation laser and collection objective lens above the sample plane, thus the sample would not need to be transparent.

These TERS results show that nanoscale-resolution Raman imaging is possible for graphene, effectively enabling chemical, structural and electrical characterisation on the nanometre length-scale. TERS also extends the ability of Raman spectroscopy to investigate this exciting 2-D material with an improved lateral resolution of more than one order of magnitude. Nanoscale chemical imaging will benefit applications in many other areas of research as well, areas where improvements in understanding and characterisation have the potential to impact the quality of life substantially, such as photovoltaics, nanocomposites and catalysis.

Disclosures

The authors have nothing to disclose.

Acknowledgements

AJP, NK and DR gratefully acknowledge funding from the Innovation R&D Programme of the National Measurement System (NMS) (Project no. 115948) in the UK, and NK and DR acknowledge funding from the NEW02 Raman metrology project of the European metrology research program (EMRP).

WS gratefully acknowledges the financial support from Natural Science Foundation of China (Grant No: 61306115) and China Postdoctoral Science Foundation (Granted No. 2013M541807). WS is also thankful to the National Physical Laboratory (UK) for their hospitality.

References

1. Geim, A.K. and Novoselov, K.S., The rise of graphene. *Nature Mater.* **6** 183-191, DOI: 10.1038/nmat1849, (2007).
2. Geim, A.K., Graphene: Status and Prospects. *Science.* **324** (5934), 1530-1534, DOI: 10.1126/science.1158877, (2009).
3. Novoselov, K.S., Falko, V.I., Colombo, L., Gellert, P.R., Schwab, M.G., and Kim, K., A roadmap for graphene. *Nature.* **490** (7419), 192-200, DOI: 10.1038/nature11458, (2012).
4. Novoselov, K.S., *et al.*, Two-dimensional atomic crystals. *PNAS.* **102** (30), 10451-10453, DOI: 10.1073/pnas.0502848102, (2005).
5. Dean, C.R., *et al.*, Boron nitride substrates for high-quality graphene electronics. *Nat Nano.* **5** (10), 722-726, DOI: 10.1038/nnano.2010.172, (2010).
6. Coleman, J.N., *et al.*, Two-Dimensional Nanosheets Produced by Liquid Exfoliation of Layered Materials. *Science.* **331** (6017), 568-571, DOI: 10.1126/science.1194975, (2011).
7. Lee, C., Wei, X., Kysar, J.W., and Hone, J., Measurement of the Elastic Properties and Intrinsic Strength of Monolayer Graphene. *Science.* **321** (5887), 385-388, DOI: 10.1126/science.1157996, (2008).
8. Mayorov, A.S., *et al.*, Micrometer-Scale Ballistic Transport in Encapsulated Graphene at Room Temperature. *Nano Lett.* **11** (6), 2396-2399, DOI: 10.1021/nl200758b, (2011).
9. Ferrari, A.C. and Basko, D.M., Raman spectroscopy as a versatile tool for studying the properties of graphene. *Nat Nano.* **8** (4), 235-246, DOI: 10.1038/nnano.2013.46, (2013).
10. Malard, L.M., Pimenta, M.A., Dresselhaus, G., and Dresselhaus, M.S., Raman Spectroscopy in Graphene. *Phys. Rep.* **473** (5–6), 51-87, DOI: 10.1016/j.physrep.2009.02.003, (2009).

11. Ferrari, A.C., *et al.*, Raman spectrum of graphene and graphene layers. *Phys. Rev. Lett.* **97** (18), 187401, DOI: 10.1103/PhysRevLett.97.187401, (2006).
12. Pollard, A.J., *et al.*, Formation of monolayer graphene by annealing sacrificial nickel thin films. *J. Phys. Chem. C.* **113** 16565-16567, DOI: 10.1021/jp906066z, (2009).
13. Huang, M., Yan, H., Heinz, T.F., and Hone, J., Probing Strain-Induced Electronic Structure Change in Graphene by Raman Spectroscopy. *Nano Lett.* **10** (10), 4074-4079, DOI: 10.1021/nl102123c, (2010).
14. Mohr, M., Maultzsch, J., and Thomsen, C., Splitting of the Raman 2D band of graphene subjected to strain. *Phys. Rev. B.* **82** (20), 201409, DOI: 10.1103/PhysRevB.82.201409, (2010).
15. Ferrari, A.C., Raman spectroscopy of graphene and graphite: Disorder, electron–phonon coupling, doping and nonadiabatic effects. *Solid State Commun.* **143** (1–2), 47-57, DOI: 10.1016/j.ssc.2007.03.052, (2007).
16. Cancado, L.G., *et al.*, Quantifying Defects in Graphene via Raman Spectroscopy at Different Excitation Energies. *Nano Lett.* **11** (8), 3190-3196, DOI: 10.1021/nl201432g, (2011).
17. Das, A., *et al.*, Monitoring dopants by Raman scattering in an electrochemically top-gated graphene transistor. *Nat Nano.* **3** (4), 210-215, DOI: 10.1038/nnano.2008.67, (2008).
18. Kalbac, M., Reina-Cecco, A., Farhat, H., Kong, J., Kavan, L., and Dresselhaus, M.S., The Influence of Strong Electron and Hole Doping on the Raman Intensity of Chemical Vapor-Deposition Graphene. *ACS Nano.* **4** (10), 6055-6063, DOI: 10.1021/nn1010914, (2010).
19. Nair, R.R., *et al.*, Fluorographene: A Two-Dimensional Counterpart of Teflon. *Small.* **6** (24), 2877-2884, DOI: 10.1002/smll.201001555, (2010).
20. Krauss, B., Lohmann, T., Chae, D.H., Haluska, M., von Klitzing, K., and Smet, J.H., Laser-induced disassembly of a graphene single crystal into a nanocrystalline network. *Phys. Rev. B.* **79** (16), 165428, DOI: 10.1103/PhysRevB.79.165428, (2009).
21. Schmid, T., Opilik, L., Blum, C., and Zenobi, R., Nanoscale Chemical Imaging Using Tip-Enhanced Raman Spectroscopy: A Critical Review. *Angew. Chem. Int. Ed.* **52** (23), 5940-5954, DOI: 10.1002/anie.201203849, (2013).
22. Zhang, R., *et al.*, Chemical Mapping of a Single Molecule by Plasmon-Enhanced Raman Scattering. *Nature.* **498** (7452), 82-86, DOI: 10.1038/nature12151, (2013).
23. Su, W. and Roy, D., Visualizing Graphene Edges Using Tip-Enhanced Raman Spectroscopy. *J. Vac. Sci. Technol. B.* **31** (4), DOI: 10.1116/1.4813848, (2013).
24. Stadler, J., Schmid, T., and Zenobi, R., Nanoscale Chemical Imaging of Single-Layer Graphene. *ACS Nano.* **5** (10), 8442–8448, DOI: 10.1021/nn2035523, (2011).
25. Binnig, G., Rohrer, H., Gerber, C., and Weibel, E., Surface Studies by Scanning Tunneling Microscopy. *Phys. Rev. Lett.* **49** 57-61, DOI: 10.1103/PhysRevLett.49.57, (1982).
26. Binnig, G., Quate, C.F., and Gerber, C., Atomic force microscope. *Phys. Rev. Lett.* **56** 930-933, DOI: 10.1103/PhysRevLett.56.930, (1986).
27. Ichimura, T., Fujii, S., Verma, P., Yano, T., Inouye, Y., and Kawata, S., Subnanometric near-field Raman investigation in the vicinity of a metallic nanostructure. *Phys. Rev. Lett.* **102** (18), 186101, DOI: 10.1103/PhysRevLett.102.186101, (2009).
28. Kharintsev, S.S., Hoffmann, G.G., Dorozhkin, P.S., de With, G., and Loos, J., Atomic force and shear force based tip-enhanced Raman spectroscopy and imaging. *Nanotechnology.* **18** (31), 315502, DOI: 10.1088/0957-4484/18/31/315502, (2007).
29. Roy, D., Williams, C.M., and Mingard, K., Single-crystal gold tip for tip-enhanced Raman spectroscopy. *J. Vac. Sci. Technol. B.* **28** (3), 631-634, DOI: 10.1116/1.3425630, (2010).
30. Williams, C. and Roy, D., Fabrication of gold tips suitable for tip-enhanced Raman spectroscopy. *J. Vac. Sci. Technol. B.* **26** (5), 1761, DOI: 10.1116/1.2981078, (2008).
31. Ogawa, Y., Toizumi, T., Minami, F., and Baranov, A.V., Nanometer-scale mapping of the strain and Ge content of Ge/Si quantum dots using enhanced Raman scattering by the tip of an atomic force microscope. *Phys. Rev. B.* **83** (8), 081302, DOI: 10.1103/PhysRevB.83.081302, (2011).
32. Yeo, B.S., Schmid, T., Zhang, W.H., and Zenobi, R., Towards rapid nanoscale chemical analysis using tip-enhanced Raman spectroscopy with Ag-coated dielectric tips. *Anal. Bioanal. Chem.* **387** (8), 2655-2662, DOI: 10.1007/s00216-007-1165-7, (2007).
33. Hayazawa, N., Yano, T., and Kawata, S., Highly reproducible tip-enhanced Raman scattering using an oxidized and metallized silicon cantilever tip as a tool for everyone. *J. Raman Spectrosc.* **43** (9), 1177-1182, DOI: 10.1002/jrs.4032, (2012).
34. Dorn, R., Quabis, S., and Leuchs, G., Sharper Focus for a Radially Polarized Light Beam. *Phys. Rev. Lett.* **91** (23), 233901-233904, DOI: 10.1103/PhysRevLett.91.233901, (2003).
35. Zhang, D., *et al.*, Nanoscale Spectroscopic Imaging of Organic Semiconductor Films by Plasmon-Polariton Coupling. *Phys. Rev. Lett.* **104** (5), DOI: 10.1103/PhysRevLett.104.056601, (2010).

